

# Direct Dose Confirmation of Quantitative Autoradiography with Micro-TLD Measurements for Radioimmunotherapy

Max H. Griffith, Ellen D. Yorke, Barry W. Wessels,  
Gerald L. DeNardo, and William P. Neacy

*Division of Radiation Oncology and Biophysics, The George Washington University Medical Center, Washington, DC; Department of Nuclear Medicine, University of California, Davis, Sacramento, California; E. I. duPont de Nemours and Co., Inc., Immunopharmaceutical Research and Development, North Bilerica, Massachusetts*

Autoradiography has shown marked heterogeneous distribution of radioactivity in all ten radiolabeled monoclonal antibody/tumor combinations evaluated by our laboratories for radioimmunotherapy (RIT) in mice. Quantitative autoradiography was performed on two of these combinations ( $^{131}\text{I}$ -B72.3/colorectal carcinoma and  $^{131}\text{I}$ -LYM-1/Raji B-cell lymphoma) to obtain a correlation of film density with radiolabeled antibody distribution. Through the use of sectioned mini-thermoluminescent dosimeter(s) (TLD) or micro-TLD, isodose curves were generated from the film gradient density lines. A computer program was written to compare theoretical absorbed dose calculations to measured micro-TLD values. First-order agreement was reached for both antibody/tumor systems: (a) B72.3/colorectal system—810 cGy measured/824 cGy calculated per 200  $\mu\text{Ci}$  injected and (b) LYM-1/lymphoma system—1,740 cGy measured/1,580 cGy calculated per 656  $\mu\text{Ci}$  injected (1 cGy = 1 rad). Additionally, the measured absorbed dose heterogeneity over a 500- $\mu\text{m}$  length of up to 400% which suggests that the use of quantitative autoradiography is necessary in order to correctly determine the underlying radiobiological effects of RIT. Theoretical computer modeling based on similar autoradiographic activity distributions has also provided a convenient means of assessing absorbed dose variation patterns from other radiolabels such as  $^{90}\text{Y}$ .

J Nucl Med 29:1795-1809, 1988

Autoradiography has been shown to be a useful method in the qualitative assessment of activity distribution for radioimmunodiagnosics and radioimmunotherapy (RIT) (1-2). Quantitative methods based on scanning film densitometry (3-4) have also been attempted to spatially determine activity deposition in the hope of ultimately obtaining isodose patterns of the absorbed radiation dose. Although there is a proportional relationship between activity distribution and the local absorption of radiation dose, quantitation of absorbed doses through computational techniques can be difficult. These difficulties include: (a) the entry of large amounts ( $10^2$ - $10^3$  voxels per slice) of serially sectioned slice array data which must be spatially matched to the maximum beta range; (b) computer generated absorbed

dose values through numeric integration of point source functions over all the activity voxels; and (c) the inability to follow the variation of activity over time in the tumor and thus arrive at the true cumulated activity. Note that an autoradiograph represents a simple "freeze-frame" of activity distribution in time. The accumulation and subsequent loss of activity may be at best inferred from autoradiographs taken at different times from similar animal models. This inference results in the loss of the specific information relating to the activity distribution around unique tumor vasculature.

In recent years, our laboratory has investigated the use of mini-thermoluminescent dosimeter(s) (TLD) for the quantitation of radiation absorbed dose from RIT in animals and phantom models (5-6). A modification of this technique (7-8) has been shown to be useful in the measurement of absorbed dose in serial tumor slices of 20  $\mu\text{m}$  thickness. Although the micro-TLD method only measures absorbed dose at a point (or points) in a

Received Dec. 17, 1987; revision accepted July 11, 1988.

For reprints contact: Barry W. Wessels, PhD, Div. of Radiation Oncology & Biophysics, The George Washington University Medical Center, 901 23rd St., N.W., Washington, DC 20037.

tumor section, the total time history of the activity profile is recorded by the TLD as absorbed dose. Furthermore, the TLD measures absorbed dose not only from the planar autoradiographic section, but also from the activity distributions above and below the slice. As long as the range of the beta particulate radiation is substantially longer [e.g., iodine-131 ( $^{131}\text{I}$ ), yttrium-90 ( $^{90}\text{Y}$ ), rhenium-186 ( $^{186}\text{Re}$ )] than the average transverse dimensions of the TLD ( $200\ \mu\text{m} \times 400\ \mu\text{m}$ ), marked disruption to the electronic equilibrium conditions in the media by the TLD detector is not evident (6). Further it has been shown in phantom studies (6) that no angular dependence of TLD orientation relative to the medium is detectable. As previously stated, it is also feasible to calculate absorbed dose by using a computational method based on a three-dimensional array of activities obtained from quantitative autoradiography of a tumor slice. The main purpose of this publication is to compare micro-TLD measurements and corresponding computerized dosimetry calculations using actual RIT tumor models and autoradiographs.

It is further proposed that implanted micro-TLD can be used to calibrate the autoradiographic activity distribution in terms of absorbed dose. This combined method avoids the use of complex data entry and point source function computer calculations to generate isodose lines for slowly varying activity distributions along the microtome sectioning axis. The combined method offers a suitable and labor saving solution for the computational difficulties that exist when autoradiography is used alone as the basis to calculate absorbed dose distributions.

## MATERIALS AND METHODS

### TLD Implantation and Animal Biodistribution Data

The miniature  $\text{CaSO}_4:\text{Dy}$  TLD technique was used as a starting point for the autoradiography/micro-TLD experiments presented here and has been described elsewhere (5-6). Rod-shaped dosimeters with dimensions of  $200\ \mu\text{m} \times 400\ \mu\text{m} \times 5,000\ \mu\text{m}$  were implanted into tumor-bearing athymic nude mice undergoing radioimmunotherapy. LS174T colorectal and Raji B-cell lymphoma-bearing mouse models (Immunopharmaceutical R & D, E.I. duPont de Nemours and Co., Inc., and the University of California-Davis, respectively) were used. Typically, eight anatomic sites per mouse were implanted as described previously (9). In addition, the tumor site received two TLD implants. Within 24 hr after TLD implantation,  $^{131}\text{I}$ -labeled B72.3 or Lym-1 monoclonal antibody was injected intravenously into the tail vein of mice with colorectal or Raji B-cell tumors, respectively. Tissue and organ samples for biodistribution studies were obtained at time of killing. Figures 1 and 2 are average biodistribution results tabulated from tumor-bearing mice receiving similar amounts and activities of the radiolabeled antibody which were then killed at approximately the same time as the individual mice used in the micro-TLD experiments. A more detailed pres-

entation of these animal tumor models and antibody preparation may be found in previous publications (2,10,11). Specific data related to the tumor uptake of activity for the micro-TLD experiments is shown in Table 1. For the micro-TLD experiments, one colorectal tumor bearing mouse was killed after 17 days and one Raji B-cell tumor xenograft was terminated at 7 days postinjection. Within 2 hr after sacrifice, each tumor was weighed and counted for  $^{131}\text{I}$  activity (Table 1). The tumors with TLD in place were removed, quickly frozen in liquid nitrogen and immediately shipped on dry ice from our collaborators to George Washington University Medical Center for micro-TLD analysis. Dosimeters located in the other organs were also recovered and used to compute the dose enhancement factor ( $\beta$ ) for the tumor/antibody combination as previously defined (9).

### Micro TLD Fabrication

Approximately 24-48 hr after tumor excision (shipping and receiving time), the frozen tumors (one colorectal and one Raji B-cell) were cut in half using a tissue microtome knife at George Washington. Half of each tumor with TLD in situ was used to score tumor biodistribution data. The remainder of the tumor was placed in a cryostat for sectioning (Fig. 3). Each section was cut to  $20\ \mu\text{m}$  thick and contained the sectioned TLD in the original spatial location. This new technique produced micro-TLD chips with dimensions of  $20\ \mu\text{m} \times 200\ \mu\text{m} \times 400\ \mu\text{m}$  from the implanted mini-TLD. Each individual micro-TLD was removed for counting after the tissue sections were air dried for ~1 hr. The readings from these micro-TLD chips provided dose quantitation at the multicellular level.

### Micro-TLD Structural Uniformity Verification

Structural uniformity of the micro-TLD was verified by both direct microscopic observation and indirectly by measurements of light output after a standard irradiation. First, a standard miniature TLD ( $200\ \mu\text{m} \times 400\ \mu\text{m} \times 5,000\ \mu\text{m}$ ) was placed in a paraffin block and tissue sectioned into  $20\text{-}\mu\text{m}$  slices. Each sectioned micro-TLD was pulled from the paraffin slice and cleaned in alcohol or luke warm water for 30 min or less. These micro-TLD were then placed under a 20 power dissecting microscope for viewing (Fig. 4). Surface variation was scored to be  $<\pm 15\%$  over each dimension by photomicrograph analysis. Indirect verification of spatial uniformity may also be inferred from calibration experiments conducted with the micro-TLD. Four standard miniature TLD were exposed uniformly to a 4 MV x-ray radiation dose of 1,000 cGy before being placed in a paraffin block. Each miniature TLD was completely sectioned producing 250 micro-TLD ( $5,000\ \mu\text{m}$  length/ $20\ \mu\text{m}$  slices). Approximately 10 micro-TLD were randomly selected from each of the four mini-TLD for counting of light output. One of the four data sets is shown in Figure 5 which is typical of these sectioned TLD rods. The standard error of this data set was measured to be  $\pm 10\%$  with an average signal of  $4.095 \pm 0.400\ \text{nC}$ . Background signal for these micro-TLD was  $0.11 \pm 0.015\ \text{nC}$ .

### Micro TLD Degradation Experiment

Since the grain size ( $40\text{-}50\ \mu\text{m}$ ) of the TLD material was similar to the slice thickness ( $20\ \mu\text{m}$ ), degradation of the teflon imbedded TLD material versus time in varying acid/base solutions was examined. Five micro-TLD per experimental

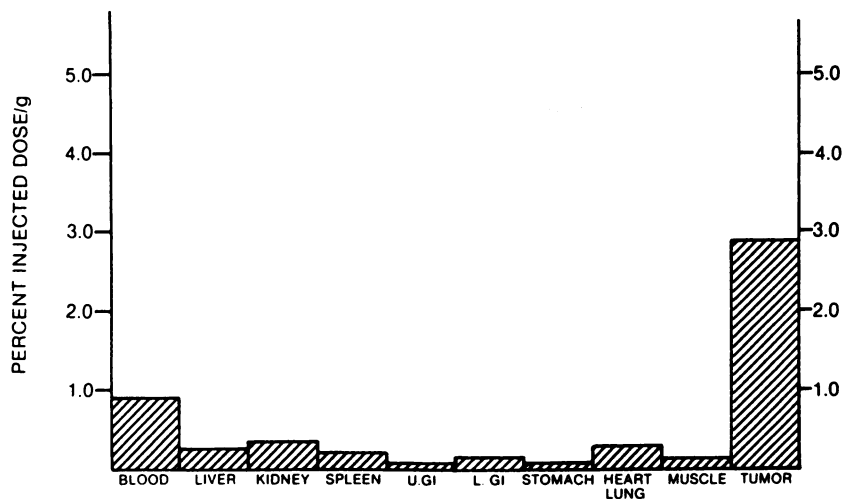


**FIGURE 1**  
Average biodistribution data for colorectal mouse xenograft (n = 6). This graph shows percent injected dose/g vs. organ site containing  $^{131}\text{I}$  labeled B72.3 antibody. Time of death was 17 days.

point were irradiated with 4 MV x-rays to a dose of 200 cGy and suspended in water solutions of pH ranging from 5 to 11 for times ranging from 2 min to 168 hr. A total of five different time periods in aqueous solutions of six different pH values were measured. Results indicated the TLD material did not suffer degradation while exposed to an acid/base environment within the limits of experimental error ( $\pm 10\%$ ).

#### Autoradiography

Autoradiographic film (LKB-Produkter AB, Bromma, Sweden) without a low energy absorbing supercoating was selected for the autoradiography experiments. The absence of this "anti-scratch" layer made this film sensitive to both high and low energy beta rays (12). A thorough dehydration of each tissue section was necessary prior to autoradiography. Immediately after fixing the frozen sections on glass slide covers, they were allowed to dry and then mounted to a thin cardboard sheet cut to fit inside an 8 in.  $\times$  10 in. film cassette. The film was placed emulsion side down on the tissue sections and the cassette was closed with the film in firm contact with each slide. Exposure times were adjusted depending upon average tumor specific activity. The times were based upon previous experiments in which test films of tissue sections were exposed for times ranging from 1 to 168 hr.

The autoradiographic film was developed in a commercial developer (Kodak D170, Rochester, NY) at 20°C for 5 min, fixed in sodium thiosulfate at 20°C for 5 min and washed in water for 10 min. Spatial resolution of the autoradiographic patterns, as confirmed by microscopic evaluation of a high contrast activity step function, was on the order of 10–50  $\mu\text{m}$  when using  $^{131}\text{I}$  or  $^{90}\text{Y}$  radiolabeled sources (data not shown).

#### Densitometry

The optical density (O.D.) was measured using an automated micro-densitometric device (developed by Loats Associates, Inc., Westminster, MD and marketed by Amersham Corporation, Arlington Heights, IL) capable of measuring optical density with 20  $\mu\text{m}$  pixel resolution. Autoradiographic images were entered into this device through a video digitizing subsystem. Software supplied by the manufacturer permitted the recording of optical density profiles along selected lines of interest (Fig. 6). A set of square grids of optical densities were obtained by measuring optical density profiles along a series of parallel lines on the autoradiographs of interest. These provided the raw data for the calculations.

#### Conversion of Optical Density to Activity

To convert the optical density values to cumulated activities, a calibration curve for the autoradiographic film exposed

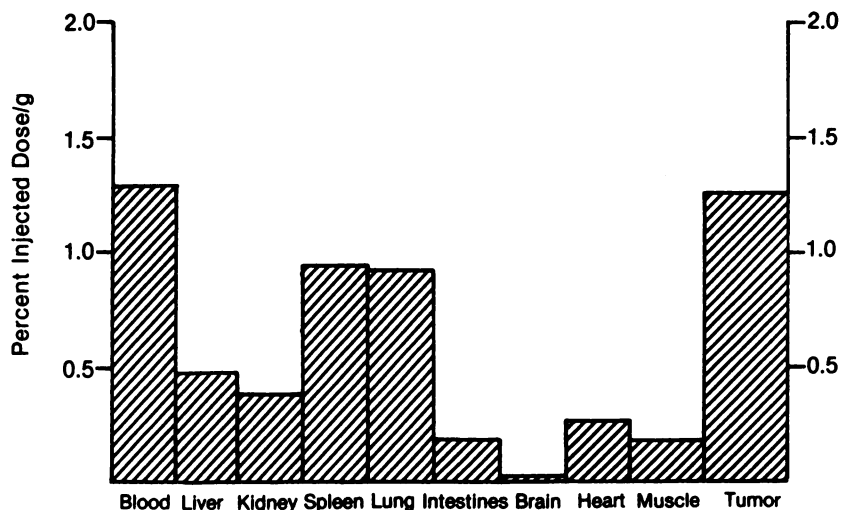


**FIGURE 2**  
Average biodistribution data for a Raji B-cell lymphoma mouse xenograft (n = 4). The plot shows percent injected dose/g vs. organ site containing  $^{131}\text{I}$ -labeled LYM-1 antibody. Time of death was 6 days.

**TABLE 1**  
Antibody/Tumor Parameters

Tumor Model/Antibody	Colorectal: B72.3	Lymphoma: LYM-1
Animal weight (g)	27.0	25.0
Amount of antibody injected-activity ( $\mu\text{Ci}$ )	200.0	656.0
Protein ( $\mu\text{g}$ )	16.3	21.5
Antibody immunoreactivity (%)	11.0	53.0
Tumor weight (mg)	1052.0	496.0
Tumor activity ( $\mu\text{Ci}$ )	2.1 (8.9) <sup>*</sup>	1.2 (2.2) <sup>*</sup>

<sup>\*</sup> Decay corrected to time of injection

to  $^{131}\text{I}$  was obtained. Film strips were exposed to gel wafers (200  $\mu\text{m}$  thick) having  $^{131}\text{I}$  specific activities ranging from 0.1 to 100  $\mu\text{Ci/g}$ . Exposure times were varied from 3 to 168 hr and a calibration curve (Fig. 7) was obtained. This calibration curve was used to convert grids of optical density values to corresponding grids of cumulated activities over the duration of TLD implantation by making two corrections. The first, a purely physical correction, accounted for the difference in thickness between the calibration wafer and the tissue slice. The second correction was a back decay of activity to account for the time course of activity during the TLD implant. For simplicity, we chose to use a steady-state assumption regarding accumulation and release of activity by the tumor in vivo. Both of these corrections are discussed in detail in Appendix A.

Alternatively, the TLD themselves were used to calibrate the autoradiographs from a single tumor. Two micro-TLD, one from a high O.D. and one from a low O.D. region of the

tumor were chosen. Both optical densities lay on a near linear portion of the calibration curve. The absorbed dose received by each TLD was recorded. The cumulated specific activity in the region surrounding the TLD was assumed to be that which would deliver the recorded absorbed dose to the TLD in an infinite uniform medium where an equilibrium dose constant calculation (13-15) would be valid. A basically linear relationship was found between film density and cumulated specific activity. This relationship was used to infer the cumulated activity distribution throughout the tumor. An example is shown in detail in Appendix B.

Since the TLD measured total absorbed dose, effectively integrating over time, no biologic model for the time dependence of activity need be assumed if they are used to calibrate the autoradiographs. However, an approximation is implicit in the use of an infinite medium calculation to estimate the cumulated activity in the neighborhood of the TLD. To minimize the effect of this approximation, the TLD should be selected from regions where the optical density gradient is small.

#### Calculation of Absorbed Dose

The absorbed dose at a point of interest can be calculated analytically only for a few highly symmetric activity distributions (uniform sphere, infinite medium, infinite planar slab, etc.). For nonsymmetric distributions such as we observed with autoradiography, numerical evaluation is necessary.

We have approximated an activity-bearing volume by a three-dimensional cubic grid in which each cubic voxel contains a cumulated specific activity which may be derived from the autoradiographs as described above. The absorbed dose delivered by the activity in a voxel to a point of interest is proportional to the product of the activity and a point source function. The point source function depends on the beta spectrum and on the distance from the voxel to the calculation point. A BASIC program which runs on a personal computer (IBM Model XT Personal Computer, Armonk, NY) was written to sum the dose contributions from each voxel to a point of interest. This approach is more thoroughly discussed in Appendix C.

The point source function we chose allows the program to be used for beta emitters other than  $^{131}\text{I}$  by changing only three parameters. Thus the dose distributions generated by different radionuclides distributed with the same geometric pattern can be compared through computer modeling.

#### Verification of Computer Calculation

A test case of an infinite medium (i.e., medium large compared to the maximum range) with a uniform cumulated

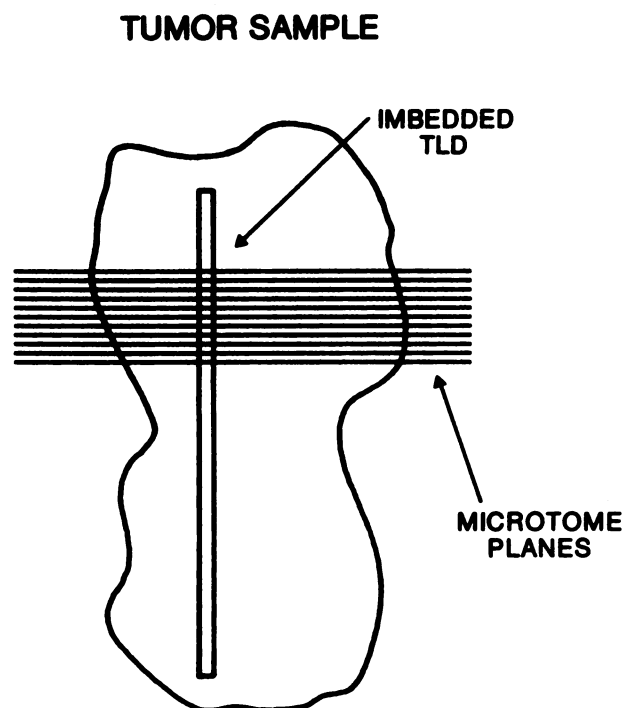


**FIGURE 3**  
Schematic representation of a sectioned tumor sample with imbedded TLD. Microtome cuts were 20  $\mu\text{m}$  thick which produced a 20  $\mu\text{m}$   $\times$  200  $\mu\text{m}$   $\times$  400  $\mu\text{m}$  TLD chip.

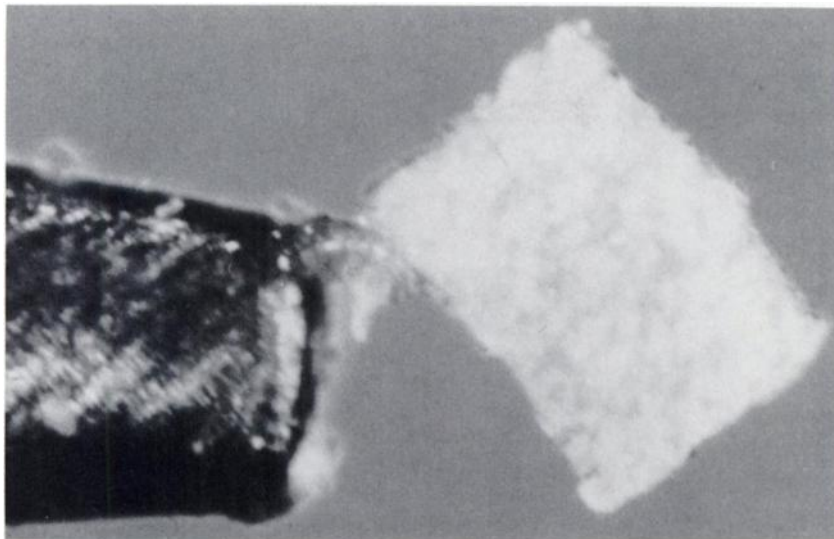


**FIGURE 4**  
Micro-TLD ( $20\ \mu\text{m} \times 200\ \mu\text{m} \times 400\ \mu\text{m}$ ) shown on the tip of microfine jeweler's tweezers. Surface variation was estimated to be  $\pm 15\%$  over each dimension.

activity was used to establish the voxel size. A compromise had to be reached between accuracy on the one hand and speed of calculation and ease of data input on the other. For an infinite uniform cumulated specific activity distribution  $C$  of  $^{131}\text{I}$ , exact calculations (13-15) predict an equilibrium dose constant of  $0.41\ \text{g-cGy}/\mu\text{Ci-hr}$  and an absorbed dose of  $0.41\ C\ \text{cGy}$  to any point in the medium. The program described above calculated a dose of 87% of the exact value with voxels which are  $200\ \mu\text{m}$  on a side and a  $15 \times 15 \times 10$  voxel grid. Reducing the length of the voxel side to  $100\ \mu\text{m}$  improved the calculation's accuracy to 93% of the exact value. In the interest of computational speed, the calculations based on actual tumor sectioned autoradiography (Figs. 8 and 9) were performed with  $200\ \mu\text{m}$  voxel side length.

Both biologic time dependencies and spatial heterogeneity are important factors in the absorbed dose measured by the micro-TLD. To test the computational approach against measurements for heterogeneous activity distributions where biologic time variations are not a consideration, comparisons were made with TLD measurements in cylindrical phantoms filled with gels of uniform activity. The experiments were

described in the literature by Wessels and Griffith (6). Figure 10 shows the agreement between the published data and the doses calculated by the program for a 3.5 mm diameter cylinder with uniform P-32 activity. The phantom radius is smaller than the phosphorus-32 ( $^{32}\text{P}$ ) beta maximum range. Thus an infinite medium calculation based upon the equilibrium dose constant of  $^{32}\text{P}$  ( $\Delta(\text{P-32}) = 1.48\ \text{g-cGy}/\mu\text{Ci-hr}$ ) seriously overestimates the dose even at the center of the cylinder, as shown by the horizontal line of Figure 10.

## RESULTS

### Autoradiography and Micro-TLD Measurements

Autoradiographic and micro-TLD data obtained from the two tumor models previously described represented typical patterns of activity and radiation absorbed dose distributions for these systems. Figures 8 and 9 show micro-TLD locations and absorbed dose readings in conjunction with the autoradiographs for

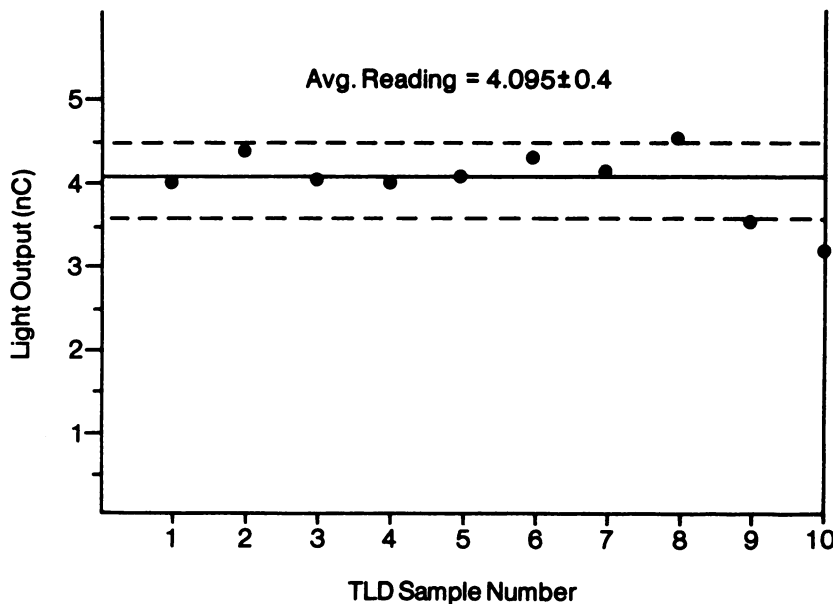


**FIGURE 5**  
Micro-TLD/4 MV x-ray uniformity results using micro-TLD ( $20\ \mu\text{m} \times 200\ \mu\text{m} \times 400\ \mu\text{m}$ ) sectioned from a mini-TLD ( $200\ \mu\text{m} \times 400\ \mu\text{m} \times 5,000\ \mu\text{m}$ ). An absorbed dose of 1,000 cGy was delivered under full buildup conditions to the mini-TLD prior to sectioning. Background signal was  $0.11 \pm 0.015\ \text{nC}$ .

**Plot of Optical Density Values Along a Cursored Line of Interest**  
 Image: Slice from Raji B-cell Lymphoma Tumor Containing I-131 Labeled LYM-1 MCA

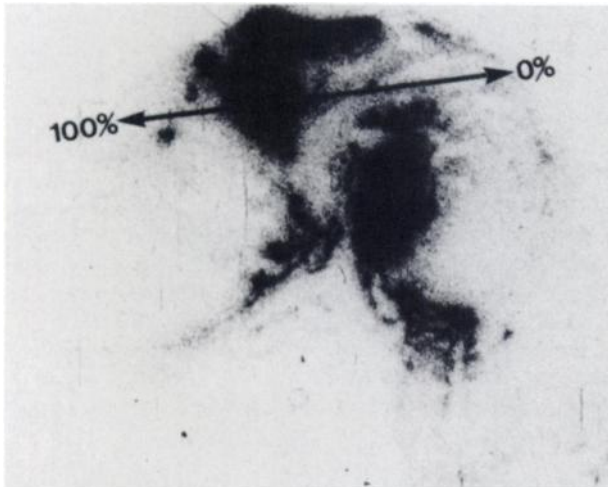
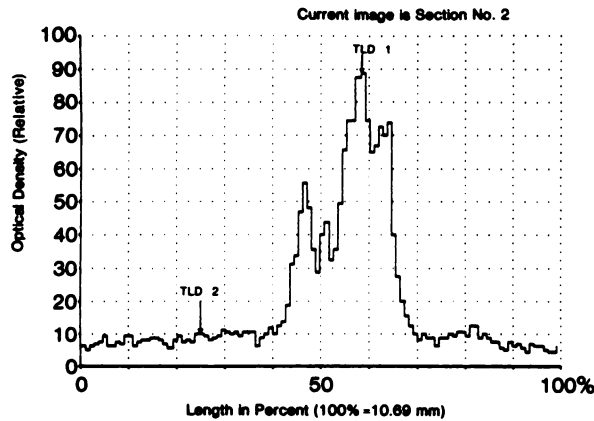


**FIGURE 6**  
 Plot of optical density values along a cursored line of interest. This autoradiographic image was taken on a slice from the Raji B-cell lymphoma tumor model containing  $^{131}\text{I}$ -labeled LYM-1 monoclonal antibody. The straight cursored line of interest passed directly over both TLD providing an activity distribution which can be correlated with micro-TLD readings.

ten sequential slices ( $20\ \mu\text{m}$  thickness) from each tumor model. Sequential autoradiographic slices for a  $1,000\ \mu\text{m}$  length of the colorectal tumor are shown in Figure 8. Despite a more homogeneous dispersion of activity than observed in the Raji B-cell data (Fig. 9), absorbed dose measurements varied by a factor of  $\sim 250\%$  ( $330\text{--}810\ \text{cGy}$ ) within this region (Slices 1–10). Single slice variation in the tumor ranged from  $175\%$  ( $470\text{--}810\ \text{cGy}$ ) for Slice 1 to  $\sim 140\%$  ( $355\text{--}505\ \text{cGy}$ ) for Slice 10. In the Raji B-cell data set (Fig. 9), TLD 1 yielded an absorbed dose variation of  $\sim 400\%$  ( $474\text{--}1,640\ \text{cGy}$ ) associated with the heterogeneous dispersion of activity within a  $500\text{-}\mu\text{m}$  microtomed region of the tumor. Additionally, a variation in absorbed dose of  $\sim 200\%$  ( $788\text{--}1,640\ \text{cGy}$ ) was noted within a single  $20\ \mu\text{m}$  tissue section as a result of the random placement of TLD 1

and 2 in regions of variable activity. Slice 1 shows the fortuitous location of TLD 1 in an area of high activity and TLD 2 in a region of lower activity.

#### Film Calibration, Activity, and Absorbed Dose Distribution: The Colorectal Tumor

The specific activity of the colorectal tumor was measured in the dose calibrator to be  $1.95\ \mu\text{Ci/g}$ . Since this tumor's autoradiographs had a more uniform film density than the Raji B-cell tumor, we compared its specific activity as derived from calibrated autoradiography with the dose calibrator measurement. The film calibration curve run for this tumor is shown in Figure 7. The average film density for the colorectal autoradiographs of Figure 8 was  $0.4\ \text{O.D.}$ . The film calibration curve was used to predict an average specific activity of  $1.51\ \mu\text{Ci/g}$  at the time of dose calibrator measurement as shown in detail in Appendix A.

Since the colorectal tumor's dimensions were relatively large compared to the  $400\ \mu\text{m}$  average range of  $^{131}\text{I}$  beta rays and the TLD placement was not close to a sharp activity gradient or to tumor edges, we compared the average absorbed dose to the micro-TLD to the absorbed dose expected in a uniform infinite medium. For this comparison, a model for the time course of the activity was needed since the TLD was embedded in tumor for 19 days prior to the beginning of autoradiography. We assumed only physical decay of  $^{131}\text{I}$  and, as shown in the last paragraph of Appendix A, calculated an absorbed dose in an equivalent infinite medium of  $600\ \text{cGy}$ . The average of the TLD readings for the tumor were  $500\ \text{cGy}$ . This agreed within  $20\%$  with the absorbed dose to an infinite medium of uniform activity equal to the average activity predicted with the use of the film calibration curve.

The computer program was also used to calculate the absorbed dose to micro-TLD A in Slice 1 of Figure 8. A volume,  $3,000\ \mu\text{m} \times 3,000\ \mu\text{m} \times 2,000\ \mu\text{m}$  surrounding the TLD and divided into voxels of side  $200\ \mu\text{m}$  were used. The physical decay of  $^{131}\text{I}$  was the only time dependence of activity considered. The contribution to the absorbed dose from the activity in slices within range of the central slice containing the micro-TLD of interest must be added to the absorbed dose due to activity in the central slice. For purposes of this estimate, it was assumed that the activity pattern of the slice containing the micro-TLD was repeated for four slices (each of thickness  $200\ \mu\text{m}$ ) above and below the central slice. We call this approximation a "cylindrical" model. The absorbed dose to the micro-TLD calculated by the program for this model was  $824\ \text{cGy}$  and was in first-order agreement with both the average infinite medium calculation of  $600\ \text{cGy}$  and the TLD reading of  $810\ \text{cGy}$ . Since biologic time dependences of activity were ignored in this calculation, disparity with the TLD measurement was not surprising.

#### TLD Calibration, Activity, and the Resultant Absorbed Dose Distributions: The Raji B-Cell Tumor

Since the Raji B-cell tumor had a very heterogeneous uptake of antibody, it was not a good candidate for use of an infinite uniform medium calculation. The TLD absorbed dose variations of  $200\%$  within a single autoradiograph slice and a  $400\%$  variation for slices which were only  $500\ \mu\text{m}$  apart were reflected in the film density as shown in Figure 9. The tumor-averaged specific activity assessed two days before autoradiography was  $2.04\ \mu\text{Ci/g}$ . No calibration curve had been run



**I-131 CALIBRATION CURVE FOR  
AUTORADIOGRAPHIC FILM  
(Cal wafer thickness = 200 microns)**

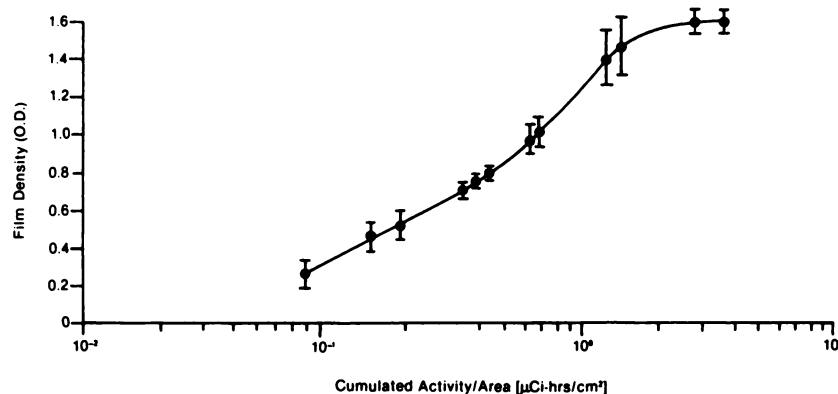


**FIGURE 7**  
Calibration curve for autoradiographic film plotting film density (O.D.) vs exposure (cumulated activity/area). The calibration wafer thickness was 200  $\mu\text{m}$  and  $^{131}\text{I}$  activities ranged from  $2 \times 10^{-3}$  to  $2 \mu\text{Ci/cm}^2$ .

in parallel to this autoradiographic sectioning experiment. Previously run film calibration curves did not necessarily apply in this case and were of limited help in quantifying this marked activity heterogeneity. However, the strong heterogeneity made this tumor an attractive candidate for the calculation of localized absorbed dose distributions. The TLD calibration of optical density described in Appendix B was used here. This procedure approximately accounted for biologically mediated time dependencies.

Figure 11 shows the calculated absorbed dose distribution based on a "cylindrical model" similar to that assumed for the colorectal tumor and based on the activity distribution surrounding TLD 1 in Slice 2. Approximately 5 min of computer time was required to obtain a typical dose pattern. Within a  $2,000 \mu\text{m} \times 2,000 \mu\text{m}$  region of interest, the calculated absorbed dose varied by a factor of 600% (260 cGy to 1,580 cGy). The average absorbed dose was 1,140 cGy with an s.d. of  $\pm 36\%$ .

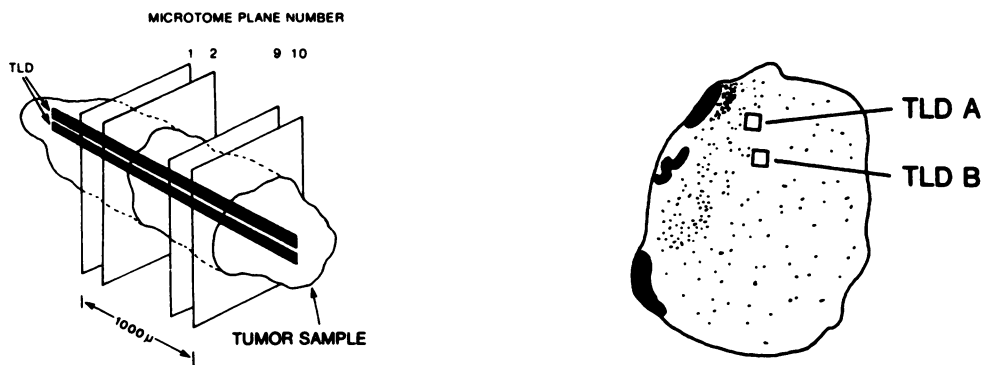
The absorbed dose pattern was not qualitatively changed if the more realistic assumption was made using activity patterns from the slices 200  $\mu\text{m}$  above and 200  $\mu\text{m}$  below the central slice. The upper slice was replicated once at 400  $\mu\text{m}$  above the center and the lower slice once at 400  $\mu\text{m}$  below the center to simulate the smaller tumor size. Although the upper and lower slices have a more homogeneous activity distribution than the central slice, a 400% variation from maximum to minimum dose was still noted within the  $2,000 \mu\text{m} \times 2,000 \mu\text{m}$  "calculation box" with a corresponding s.d. of  $\pm 30\%$ . The lower activity in the upper and lower slices as well as the shorter tumor dimensions also led to a diminished peak absorbed dose (1,110 cGy) compared to the 1,580 cGy obtained by using the cylindrical model (figure not shown). Qualitatively, the microisodose pattern is not substantially changed.







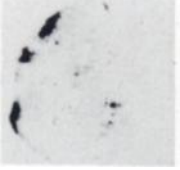
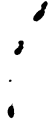


**Theoretical Modeling Using Different Radionuclides**

Existing activity patterns were used to theoretically model the effect on the absorbed dose distribution of changing the radionuclide alone. The three parameters ( $\nu$ ,  $c$ ,  $E$ ) of the point source function as described in Appendix C were appropriately

altered before rerunning the program. Figure 12 shows the absorbed dose distribution using  $^{90}\text{Y}$  parameters with the same cylindrical activity distribution that produced Figure 11 for  $^{131}\text{I}$  (Raji B-cell data set). Two effects, both attributable to the longer range of  $^{90}\text{Y}$  betas were observed. First, the absorbed dose distribution was more homogeneous for  $^{90}\text{Y}$  with a variation reduced to 250% with a mean absorbed dose of  $1,660 \pm 330$  cGy over a range of 1,100 to 2,100 cGy. Second, the peak absorbed dose of 2,100 cGy was only 26% of the 8,200 cGy which was the calculated absorbed dose to an infinite medium of uniform specific activity using the highest observed specific activity in the region. This effect was a direct result of the  $^{90}\text{Y}$  beta particle range that is relatively large compared to the tumor size and activity distribution pattern. Much of the beta energy emitted in the high activity region escaped and failed to deposit its absorbed dose within that region (lack of buildup).

As a further exercise, Figure 13 shows the effect of a hypothetical  $^{90}\text{Y}$  activity distribution with a substantially larger scale heterogeneity than that observed previously. The cumulated *specific* activity of each voxel was kept the same as in Figure 12. However, each voxel side was enlarged by a factor of 10 and consequently, the cumulated activity per cubic voxel was increased proportionally. The region over which the absorbed dose pattern was displayed was now within a  $2 \text{ cm} \times 2 \text{ cm}$  square. The size of this new region exceeded the maximum range of the  $^{90}\text{Y}$  beta particles. Hence, the maximum absorbed dose of 7,800 cGy calculated for this expanded region finally approached the expected 8,200 cGy "infinite medium" dose as full buildup of electronic equilibrium had been established. Since the high and low activity regions were more distant from each other (on the scale of the beta range), the absorbed dose heterogeneity was again as large (1,500–7,800 cGy) as in the original example (Fig. 11). To summarize, for the enlarged case the central peak absorbed dose approached the infinite medium dose and the calculated absorbed dose heterogeneity became larger whenever the length scale of heterogeneity in antibody uptake (distance between "hot spots") was comparable to or exceeded the beta

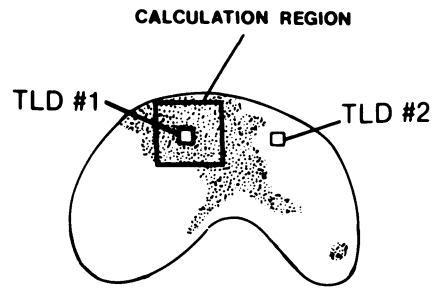
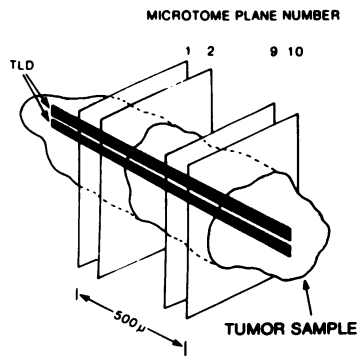


	SLICE #	TLD	DOSE (cGy)		SLICE #	TLD	DOSE (cGy)
1		A B	810 470	6		A B	620 480
2		A B	765 440	7		A B	505 345
3		A B	645 400	8		A B	500 335
4		A B	642 415	9		A B	475 330
5		A B	585 340	10		A B	505 355

\* Radiolabeled antibody and tumor model supplied by Dupont-NEN, North Billerica, Mass.

**FIGURE 8**  
 Autoradiographic results from a 1,052 mg colorectal tumor showing absorbed dose measurements which vary by 250% over a 1,000 μm region. Absorbed dose variability inside a single twenty micron tumor slice was ~175%.





	Slice #	TLD#	Dose (cGy)		Slice #	TLD#	DOSE (cGy)
1		1 2	1640 788	6		1 2	911 778
2		1 2	1740 947	7		1 2	834 697
3		1 2	1810 855	8		1 2	542 442
4		1 2	1160 735	9		1 2	500 392
5		1 2	934 797	10		1 2	474 400

**FIGURE 9**

Autoradiographic results from a 496 mg Raji B-cell tumor showing the heterogeneous distribution of activity and resulting measured TLD absorbed radiation dose. Sections 1-1 to 10-2 show a factor of 400% in absorbed dose variation associated with antibody uptake within a 500  $\mu$  region of the tumor. A variation in absorbed dose of ~200% was also noted within a single tissue section. The calculation region denoted by a 2,000  $\mu$ m  $\times$  2,000  $\mu$ m (2 mm  $\times$  2 mm) box was subdivided into an optical density grid consisting of voxels with sides 200  $\mu$ m in length.

## DOSE VS. DISTANCE FROM CENTER P-32 IN 3.5 mm DIAMETER CYLINDER

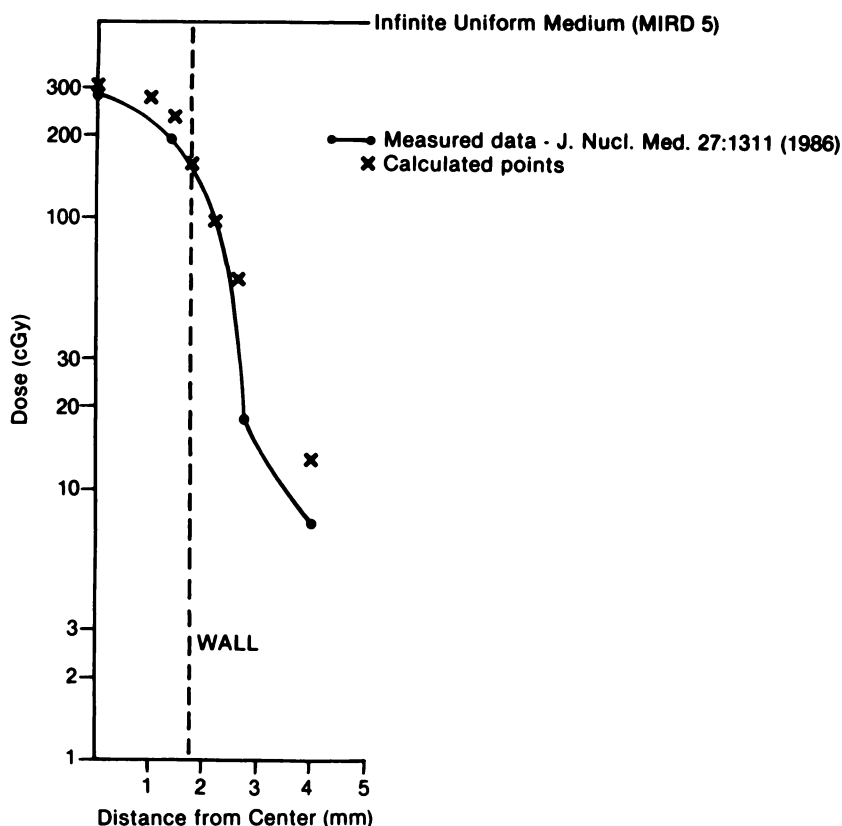


**FIGURE 10**

Absorbed dose as a function of distance from the center of a cylindrical gel tumor phantom. The inner cylinder, diameter 3.5 mm, contains  $^{32}\text{P}$  with initial concentration of 22  $\mu\text{Ci/ml}$ . The ratio of activity of the outer phantom to the inner one is 73:1. The solid curve is data measured with the miniature TLD suspended for 16 hr while the x points have been calculated using the program discussed in the text. The absorbed dose (520 cGy) calculated for infinite uniform medium would be a substantial overestimate of the absorbed dose for this small phantom.

maximum range. A comparison of all measured and calculated absorbed dose values for both antibody heterogeneity patterns using  $^{131}\text{I}$  and/or  $^{90}\text{Y}$  radiolabels is presented in Table 2.

### DISCUSSION

The results presented in Figures 8 and 9 show that the TLD implant method for assessing absorbed dose from RIT can be extended to the multicellular range (20–400  $\mu\text{m}$ ) using the newly fabricated micro-TLD to measure resulting absorbed dose heterogeneity. The accuracy and reproducibility of the measurements are limited by the dosimeter's spatial dimensions, the size of the radiation exposure (signal-to noise ratio) and the homogeneity of the detector response ( $\pm 10\%$ —Fig. 5).

Autoradiographic film calibration combined with a point source function computational method was used to assess the absorbed dose deposition in a region of mildly heterogeneous antibody uptake (Fig. 8) and was then compared with the dose to the sectioned micro-TLD in the same region. Reasonable agreement was reached (Fig. 8, Slice 1, micro-TLD—810 cGy and program results—824 cGy) between the two methods using the colorectal tumor model. In this case, the computational method was based on a standard film calibration and “freeze frame” autoradiography which

does not include biologic time dependence of the radiolabeled antibody distribution. Therefore, precise agreement with micro-TLD measurements which measure the integrated absorbed dose over time was not expected since the autoradiographic method does not account for time dependent changes in antibody concentration.

Alternatively, the micro-TLD were used to directly calibrate the isodensity lines measured from the autoradiographs. This provided a convenient general method to assess absorbed dose heterogeneity for RIT using only the isodensity autoradiograph lines calibrated by micro-TLD. This method is not expected to be extremely accurate in a region of rapid variation of antibody uptake in a plane perpendicular to the autoradiograph. In such cases, the absorbed dose to the micro-TLD reflects out-of-plane variations that are not reflected in an absorbed dose estimate based on a single autoradiographic slice. For a region of strongly heterogeneous uptake (Fig. 9), this technique also provided nominal agreement (maximum TLD measurement of 1,740 cGy as compared to program results with a maximum calculated value of 1,580 cGy). Again, the TLD measurement method is thought to reflect the actual absorbed dose to the tumor at a point and is used here as the comparison standard for the autoradiograph/computational method accuracy.

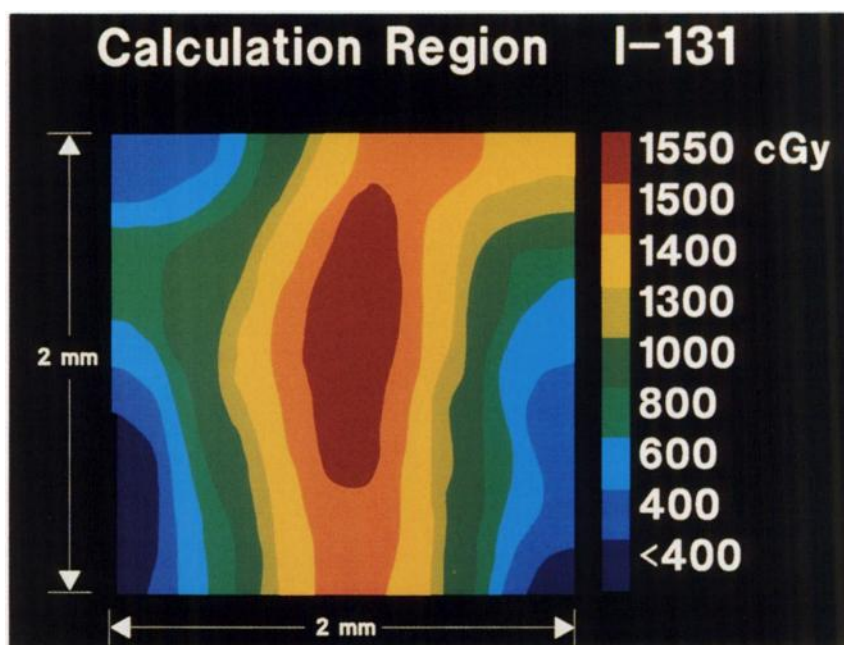


**FIGURE 11**

A micro-isodose pattern ( $^{131}\text{I}$  cylindrical model) calculated from a  $2,000\ \mu\text{m} \times 2,000\ \mu\text{m}$  region shown in Figure 9. The optical densities in the "calculation" region of Figure 9 were converted to cumulated activities using voxels with sides  $200\ \mu\text{m}$  in length. To simulate the three dimensional nature of the tumor, the activity distribution in this slice was replicated four slices above and below it. There was a variation of 600% from the high absorbed dose (1,580 cGy) to low (262 cGy) which would be obscured by simply quoting the average calculated absorbed dose of 1,140 cGy.

Lastly, Figures 11, 12, and 13 show theoretical estimates of the relative effectiveness of absorbed dose deposition for two different radionuclides in relation to the size of the heterogeneous antibody uptake pattern. In Figure 12, the region containing the maximum activity was small compared to the  $^{90}\text{Y}$  beta particle range while in Figure 13 the calculation region was expanded by a factor of ten (from 2 mm to 2 cm). In addition, a hypothetical  $^{90}\text{Y}$  activity distribution with large scale inhomogeneity was used. The resulting maximum absorbed dose increased from 2,100 to 7,800 cGy. When the activity was contained in a region which was the same size or smaller than the particle range (Fig. 12), the use of absorbed dose estimates appropriate to infinite media (equilibrium dose constant multiplied by the cumulative specific activity (15)) was not a valid approximation and yielded absorbed dose values several times too large due to the lack of an adequate buildup region.

Furthermore, when large activity variations occur over distances comparable to or larger than the particle range, the use of an infinite medium estimate obscures absorbed dose variations which are of potential radiobiological importance. These variations can occur on a scale five times smaller than the resolving power of standard nuclear medicine gamma cameras, as in the case of the experimental data cited here (Figures 8 and 9). When heterogeneous antibody uptake patterns are

on the same scale as the particle range, direct measurement techniques or computational methods based on experimentally derived activity distributions are warranted. This suggests that (a) the autoradiography/micro-TLD method or computational techniques must be performed in order to properly characterize any antibody/tumor combination and (b) a range of absorbed doses rather than a simple mean should be quoted when describing absorbed doses generated by RIT. In addition, the use of "cocktails" or a variety of radionuclides coupled to different antibodies may be appropriately selected once the size and dimensions of the heterogeneous uptake patterns is determined for a specific antibody/tumor system through the methods described above.

#### ACKNOWLEDGMENTS

The authors thank Mr. Bernard Skibinski, Ms. Naomi Miyao, and Ms. Susan Danskin for their expert technical assistance and Dan Macey, PhD for his review of the manuscript. They also thank Ms. Gloria Lester for her secretarial assistance in preparing this manuscript.

This work was partially supported by an NIH research grant #NIH2 507 RR05359-22 at The George Washington University, Washington, DC, by a U.S. Department of Energy Grant #DE FG03 84ER60233 at the University of California, Davis and research funds available from E. I. duPont de Nemours and Co., Inc., Billerica, MA.

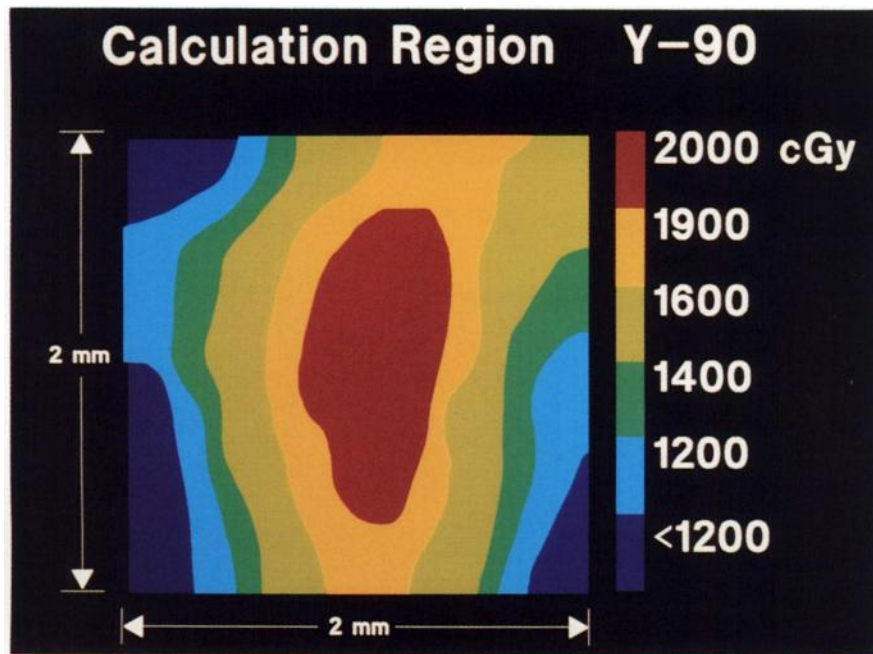


**FIGURE 12**

Theoretical micro-isodose pattern that demonstrated the effect of a change in radiolabel. The specific activity distribution used in Figure 11 was retained, but the point source function parameters appropriate to  $^{90}\text{Y}$  were incorporated.  $^{90}\text{Y}$  has a more energetic beta spectrum than  $^{131}\text{I}$  with an average range of 3–4 mm. A simple equilibrium dose constant estimate of the maximum absorbed dose predicted 8,200 cGy for the infinite medium calculation. The small tumor size reduced this value to 2,100 cGy. The longer  $^{90}\text{Y}$  range also reduced the absorbed dose variation over the calculation region to only 230%.

## APPENDIX A

The calibration curves were plotted as film density versus cumulated specific activity per unit area of the calibration wafer (Fig. 7). The film density records the absorbed dose to the film at the surface of the wafer, or of the autoradiographic slice. Equal film density in fact implies equal absorbed dose to the film at these two surfaces. Since the wafers ( $200\ \mu\text{m}$ ) are thicker than the slices ( $20\ \mu\text{m}$ ), equal surface absorbed doses are produced by a lower cumulated specific activity in the wafer than in the slice. If the slice activity distribution were uniform on the length scale set by the point source function parameter  $1/\nu$  defined in Appendix C, both wafer and slice could be approximated by infinite slabs of thickness  $h_w$  and  $h_s$  and cumulated specific activities  $C_w$  and  $C_s$ , respectively. Loevinger et al. (13) have derived a general expression for the dose at the surface of a slab of thickness  $h$ :

$$D_s = 0.5 D_\infty f(h) \quad (\text{A1})$$

where:

$$f(h) = c^2 \alpha [\nu h/c(2 + \ln c\nu h) + \exp(1 - \nu h/c) - 3] + 1 - \alpha \exp(1 - \nu h) \text{ for } \nu h < c \text{ and,}$$

$$f(h) = 1 - \alpha \exp(1 - \nu h) \text{ for } \nu h > c$$

$D_\infty$  = dose to infinite medium;  $\nu$ ,  $c$ ,  $\alpha$  are point source function parameters.

Since the absorbed dose at the surface of the wafer is equal to that at the surface of the slice:

$$C_w f(h_w) = C_s f(h_s). \quad (\text{A2})$$

Using the point source function parameters appropriate to  $^{131}\text{I}$  as discussed in Appendix C and the known thickness of wafer and slice, we find:

$$C_s = 4.16 C_w. \quad (\text{A3})$$

For the nonuniform activity distributions characteristic of the tumors we studied, the steepness of the activity gradient in the plane of the autoradiograph limits the validity of use of a uniform activity calibration wafer and the spatial resolution of the derived autoradiographic activity density information. Spatial resolution of the input data is improved somewhat by the proximity of the film (relative to the size of the grid voxel over which the activity is averaged) to the slice. Within this approximation, a map of the average cumulated specific activity within each slice voxel is obtained.

Given that the exposure time,  $T_e$ , for a slice is known, the specific activity  $A_v$  of each voxel at the beginning of the autoradiographic exposure is given by:

$$A_v = C_v \lambda / (1 - \exp(-\lambda T_e)), \quad (\text{A4})$$

where  $C_v$  is the cumulated specific activity of the voxel during the autoradiograph and  $\lambda$  is the decay constant of the beta emitter. To use these specific activities to calculate doses delivered to an implanted TLD, the history of the activity in the slice for the duration of the TLD implant must be known.

In addition to temporal information regarding when the TLD was inserted (time  $T_1$ ), and removed (time  $T_2$ ), relative to the autoradiographic procedure, either comparative experimental measurements or model assumptions must be made for the time dependent biodistribution of activity in the tumor.



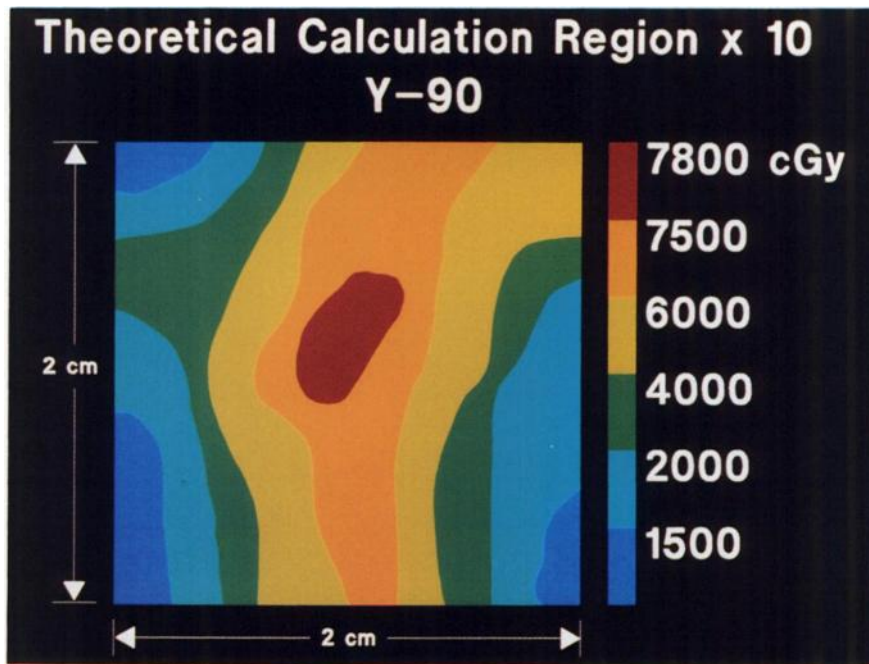


**FIGURE 13**

Theoretical micro-isodose pattern for  $^{90}\text{Y}$  utilizing a geometrically similar but expanded region for the proper absorbed dose buildup for this radionuclide. If the same specific cumulated activity was kept in each voxel, but each voxel side was multiplied by a factor of ten (region now 2 cm  $\times$  2 cm), the peak absorbed dose approached that predicted by an equilibrium dose constant calculation. Since the "hot" and "cold" regions were no longer within an adequate particle range of each other, absorbed dose inhomogeneity was sizeable (700%).

In our present calculations, it is assumed that only physical decay of activity with decay constant,  $\lambda$ , occurs for the duration of the TLD implant. Using this assumption, if the specific activity of a voxel of an autoradiographic slice at the time the autoradiograph starts is  $A_0$ , then the cumulated specific activity of that voxel for the duration of the TLD implant is given by:

$$C = A_0 \exp(\lambda T_1) (1 - \exp(-\lambda(T_1 - T_2))) / \lambda. \quad (\text{A5})$$

In a similar manner, a more refined model of antibody bio-

distribution can be used to convert the film density map to a map of the cumulated activity distribution in the slice for the duration of the TLD implant. As an example of the use of this procedure, we consider the colorectal tumor (Fig. 8) for which the average specific activity measured two days before the start of autoradiography was 1.95  $\mu\text{Ci/g}$ . Using the half-life of  $^{131}\text{I}$  as 8.02 days, the average activity (assessed from the dose calibrator measurement) at the beginning of autoradiography had decayed to 1.64  $\mu\text{Ci/g}$ . This can be compared with the average activity predicted from the use of film cali-

**TABLE 2**  
Comparison of Measure and Calculated Absorbed Dose Values

	TLD measurement maximum (cGy)	range (cGy)	Average dose point source calculations (cGy)	Range (cGy)	Uniform media peak value MIRD (cGy)
Colorectal Tumor $^{131}\text{I}$ -B72.3	810	330-810 <sup>‡</sup>	640	420-824	600
Raji B-cell Tumor $^{131}\text{I}$ -Lym-1	1740	392-1,740 <sup>‡</sup>	1,140	260-1,580 <sup>†</sup>	1,700
Raji B-cell Tumor $^{90}\text{Y}$ -Lym 1 <sup>††</sup> (Small scale heterogeneity) —Figure 12	N.A.	—	1,660	1,100-2,100	8,200
Raji B-cell Tumor $^{90}\text{Y}$ -Lym-1 <sup>††</sup> (Large scale heterogeneity) —Figure 13	N.A.	—	5,570	1,500-7,800	8,200

\* Theoretical result.

† Over calculation box only.

‡ Over all TLD sections.

N.A.—Not available.

bration of the autoradiographs. The films were exposed for 24 hr and the average film density measured was 0.4 (O.D.), corresponding to a cumulated wafer activity per area of 0.14  $\mu\text{Ci-hr/cm}^2$  or a specific cumulated activity for a unit density 200  $\mu\text{m}$  thick calibration wafer of 7  $\mu\text{Ci-hr/g}$ . Using Eq. (A3), the corresponding 20  $\mu\text{m}$  slice cumulated specific activity is 29.1  $\mu\text{Ci-hr/g}$ . Since the film was exposed for 24 hr, the tumor specific activity at the start of autoradiography (Eq. (A4) with  $T_e = 1$  day) is 1.27  $\mu\text{Ci/g}$ . The specific activity at the time of dose calibration measurement, was found by back decaying to be 1.51  $\mu\text{Ci/g}$ , agreeing with the dose calibration measurement to within  $\pm 30\%$ .

The average cumulated specific activity during TLD implantation can be calculated under the assumption of purely physical decay of  $^{131}\text{I}$  using Eq. (A5). The TLD was implanted 19 days prior to autoradiography and removed immediately before; hence  $T_1 = 19$  days and  $T_2 = 0$ . Taking  $A_0 = 1.27$   $\mu\text{Ci/g}$  and the physical half-life of  $^{131}\text{I}$ , the calculated cumulated specific activity during TLD implant is 1,469  $\mu\text{Ci-hr/g}$ . The absorbed dose to an infinite medium of this cumulated specific activity can be calculated using the equilibrium dose constant for  $^{131}\text{I}$  beta rays,  $\Delta(^{131}\text{I}) = 0.41$   $\text{g-cGy}/\mu\text{Ci-hr}$ . Using these initial values, the absorbed dose to infinite medium was calculated to be 602 cGy.

## APPENDIX B

The micro-TLD can be used to approximately calibrate autoradiography as described in Methods and Materials. This technique was used to calibrate autoradiographs for the Raji B-cell tumor where, fortuitously, TLD 1 was located in a high activity region and TLD 2 in a lower activity region.

The TLD measurement of 1,740 cGy would be achieved in an infinite medium with cumulated specific activity of 4,244  $\mu\text{Ci-hr/g}$  by the equilibrium constant method. This absorbed dose, which corresponds to Figure 9, Slice 2-TLD 1, was received by a micro-TLD embedded in a region of film density 0.79 O.D.. Similarly, micro-TLD 2 in Slice 10 in a region of film density 0.3 O.D. received a dose of 400 cGy and was associated with a cumulated specific activity of 976  $\mu\text{Ci-hr/g}$ . Both these optical densities were located in the near linear region of the calibration curve. A linear relationship was then assumed between film density and cumulated specific activity within 0.3 and 1.0 O.D. readings.

Thus, film density 0.5 O.D. would be associated with cumulated specific activity of 2,310  $\mu\text{Ci-hr/g}$  by linear interpolation.

## APPENDIX C

To calculate the absorbed dose to a point  $\bar{r}$  due to a volume distribution of specific cumulated activity  $C(\bar{r}')$ , it is necessary to have a point source function  $J(|\bar{r} - \bar{r}'|)$  specifying the absorbed dose at  $\bar{r}$  due to a unit strength point source at  $\bar{r}'$ . In unit density material, the absorbed dose at  $\bar{r}$  is given formally by the volume integral:

$$D(\bar{r}) = \int C(\bar{r}') J(|\bar{r} - \bar{r}'|) d\bar{r}'. \quad (\text{C1})$$

A number of point source functions for various beta emitters are available in the literature (13,16,17). We used the point source function of Loewinger et al. (13) which is a three parameter fit to the absorbed dose distribution of a point beta emitting source. The dose rate at a distance  $x$  from the point source is given by:

$$J(x) = \frac{K}{(\nu x)^2} \left\{ c \left[ 1 - \frac{\nu x}{c} \exp\left(1 - \frac{\nu x}{c}\right) \right] + \nu x \cdot \exp(1 - \nu x) \right\} \quad \text{for } x < \frac{c}{\nu} \quad \text{and,} \quad (\text{C2})$$

$$J(x) = \frac{K}{\nu x} \exp(1 - \nu x) \quad \text{for } x \geq \frac{c}{\nu}.$$

Here  $\nu$  and  $c$  are parameters depending upon the beta spectrum chosen to fit experimental dose distributions and  $k$  is related to the average energy  $\bar{E}$  (in MeV) of the spectrum by:

$$k = 0.17 \rho^2 \nu^3 \bar{E} / (3c^2 - c(c^2 - 1)) \text{ cGy}/\mu\text{Ci-hr}. \quad (\text{C3})$$

Values of  $\nu$ ,  $c$  and,  $\bar{E}$  are given in Reference 13 for several radionuclides; for example, for I-131,  $\nu = 40 \text{ cm}^{-1}$ ,  $c = 2$ ,  $\rho$  (density) = 1  $\text{gm/cm}^3$  and  $\bar{E} = 0.187$  MeV.

While Eq. (C1) can be analytically integrated for highly symmetric activity distributions (13), for nonsymmetric distributions numerical evaluation is necessary. We approximated the activity-bearing volume by a three-dimensional cubic grid in which each cubic voxel had volume  $V$  and was centered on a grid point  $\bar{x}_L$ . The cumulated specific activity,  $C(\bar{x}_L)$  of each voxel was input data. The integral of Equation C1 was approximated by a sum over the voxels and, in our work,  $J$  was Loewinger's point source function. However, other analytic point source functions or lookup tables such as have been compiled by Berger (18) for monoenergetic electrons could be used. We found that compiled BASIC on a personal computer generated the absorbed dose distributions discussed in the body of this paper in  $\sim 5$  min each.

## REFERENCES

1. Jones PL, Gallagher BM, Sands H. Autoradiographic analysis of monoclonal antibody distribution in human colon and breast tumor xenografts. *Cancer Immunol Immunother* 1986; 22:139-143.
2. Esteban JM, Schlom J, Mornex F, et al. Radioimmunotherapy of athymic mice bearing human colon carcinomas with monoclonal antibody B72.3: histological and autoradiographic study of effects on tumors and normal organs. *Eur J Cancer and Clin Oncol* 1987; 23:643-655.
3. Yonekura Y, Brill AB, Som P, et al. Quantitative autoradiography with radiopharmaceuticals, Part I: Digital film-analysis system by videodensitometry: concise communication. *J Nucl Med* 1983; 24:231-237.
4. Lewellen TK, Graham MM, Spence AM. Quantitative autoradiography using a personal computer. *J Nucl Med* 1986; 27:549-554.
5. Wessels BW, Bach P, Quadri, SM. Microdosimetric



- TLD measurements for tumor associated antibody therapy [Abstract]. *J Nucl Med* 1984; 25:P39.
6. Wessels BW, Griffith MH. Miniature thermoluminescent dosimeter absorbed dose measurements in tumor phantom models. *J Nucl Med* 1986; 27:1308-1314.
  7. Griffith MH, Wijewardene C, Wessels BW. Micro TLD and autoradiographic measurements for radiolabeled antibody uptake in tumor bearing mice. *Med Phys* 1985; 12:672.
  8. Neacy WP, Wessels BW, Bradley EW, et al. Comparison of radioimmunotherapy (RIT) and 4 MV external beam radiotherapy of human tumor xenografts in athymic mice. *J Nucl Med* 1986; 27:902.
  9. Wessels BW, Griffith MH, Bradley EW, et al. Dosimetric measurements and radiobiological consequences of radioimmunotherapy in tumor bearing mice. Fourth International Radiopharmaceutical Dosimetry Symposium, CONF-851113:446-457, Oak Ridge, 1985.
  10. Sands H, Jones PL. Methods for the study of metabolism of radiolabeled monoclonal antibodies by liver and tumor. *J Nucl Med* 1987; 28:390-398.
  11. Koizumi K, DeNardo GL, Denardo SJ, et al. Multi-compartmental analysis of the kinetics of radioiodinated monoclonal antibody in patients with cancer. *J Nucl Med* 1986; 27:1243-1254.
  12. Ehn E, Larsson B. Properties of an anti-scratch-layer-free x-ray film for the autoradiographic registration of tritium. *Sci Tools* 1979; 26:24-29.
  13. Loevinger R, Japha EM, Brownell GL. Discrete radioisotope sources. *Radiation Dosimetry*. In: Hine GJ, Brownell GLM, eds. New York: Academic Press, 1956: 693-799.
  14. Loevinger R, Berman M. A Revised Schema for Calculating the Absorbed Dose from Biologically Distributed Radionuclides, MIRD Pamphlet No. 1, Revised. New York: The Society of Nuclear Medicine, 1976.
  15. Dillman LT, Von der Lage FC. Radionuclide Decay Schemes and Nuclear Parameters for Use in Radiation-Dose Estimation, MIRD Pamphlet No. 10. New York: The Society of Nuclear Medicine, 1975.
  16. Prestwich WV, Chan LB, Kwok CS, et al. Dose point kernels for beta-emitting radioisotopes. Fourth International Radiopharmaceutical Dosimetry Symposium CONF-851113:545-559, Oak Ridge, 1985.
  17. Vynckier S, Wambersie A. Dosimetry of beta sources in radiotherapy, I. The beta point source dose function. *Phys Med Biol* 1982; 27:1339-1347.
  18. Berger MJ. Distribution of Absorbed Dose around Point Sources of Electrons and Beta Particles in Water and Other Media. MIRD Pamphlet #7. *J Nucl Med Suppl* 1971; 5, 5.